JOURNAL OF COMPUTATIONAL PHYSICS 78, 178–193 (1988)

Streamwise Computation of Three-Dimensional Incompressible Potential Flows

MAHESH S. GREYWALL

Department of Mechanical Engineering,
Wichita State University, Wichita, Kansas 67208

Received April 30, 1987; revised October 13, 1987

A new method for the computation of three-dimensional incompressible potential flows is presented. The dependent variables of this method are the streamwise velocity along a set of chosen streamlines, and the coordinates of the chosen streamlines in the cross-stream plane. Since the method computes streamline coordinates directly, it can be easily used to generate boundary fitted grids for the computation of three-dimensional viscous flows. Sample computations are presented for (i) flow through a rectangular diffuser with an offset and with a change in the aspect ratio, and (ii) flow through a duct whose cross section changes from a square to a rhombus. © 1988 Academic Press, Inc.

I. INTRODUCTION

Use of the stream function or the streamline coordinates for the computation of flow fields has a long and varied history. Computation of two-dimensional incompressible potential flows using the stream function as the dependent variable and the space coordinates as the independent variables is well known and can be found in almost any introductory fluid mechanics book. In the hodograph method (e.g., Shapiro [1]) equations of the potential flow are formulated using the stream and the potential functions as the dependent variables and the velocity components as the independent variables. Uchida and Yasuhara [2] and Ishii [3], for example, have calculated axisymmetric potential flow using this last set of variables. Pearson [4, 5] has used the streamline geometry in conjuntion with Euler's equations of motion to compute isentropic flows.

The stream function has also been used in the computation of viscous flows. In the recent past, the stream function, along with the vorticity, has been used extensively to compute two-dimensional incompressible viscous flows (e.g., Anderson *et al.* [6]). Patankar and Spalding [7] have used the stream function to construct the cross-stream coordinate for the computation of two-dimensional compressible "parabolic" (boundary layer) type flows. Kwon and Pletcher [8] have used the stream function and the axial velocity as the dependent variables to compute two-dimensional incompressible separated channel flow. These are a few examples of the use of the stream function for the computation of viscous flows.

0021-9991/88 $3.00

More recently, streamlines of the incompressible potential flow corresponding to a given geometry have been used to construct boundary-fitted grid systems for the computation of viscous flows. The streamlines needed for the grid generation have been calculated by various methods. For example, Ghia *et al.* (9) generated the grid by the use of conformal mapping; Meyder [10], and Ferrel and Adamczyk [11], by solving the potential equation. A survey of the use of streamlines to generate a grid is included in the review article on grid generation by Thompson *et al.* [12].

Over the past few years we have used the streamwise velocity along a set of chosen streamlines and the cross-stream coordinates of the chosen streamlines as the dependent variables to compute flow fields. Using these variables we computed two-dimensional turbulent flow in Ref. [13], and three-dimensional laminar flow through rectangular ducts in Ref. [14]. Both these studies assumed the flow to be "parabolic." In Ref. [15] we computed two-dimensional incompressible potential flows using these variables. In the present study we present the computation of three-dimensional incompressible potential flows. Since the algorithm presented computes the streamline coordinates directly, it seems well suited to the generation of a boundary-fitted grid for the computation of three-dimensional viscous flows.

II. Stream Surface Equations

Let the main flow direction be along x, and (y, z) be the coordinates of the cross-stream plane. Further, let U represent the streamwise velocity along a given streamline, and Y and Z represent the coordinates of the given streamline in the cross-stream plane. The differential equations for U, Y, and Z are (see, Ref. [15])

$$\frac{DU}{Dt} = f^s, \tag{1}$$

$$Y_{xx} = (1 + Y_x^2 + Z_x^2)(f^y - Y_x f^x)/U^2, \tag{2}$$

$$Z_{xx} = (1 + Y_x^2 + Z_x^2)(f^z - Z_x f^x)/U^2. \tag{3}$$

Equation (1) is obtained by applying Newton's second law of motion in the stream-wise direction to a fluid element. Equation (2) is obtained by projecting the motion of the fluid element on to the $x-y$ plane and then applying Newton's second law normal to the projected motion. Equation (3) is obtained similarily to Eq. (2). In Eqs. (1)–(3) the subscript x represents derivatives with respect to x in the (x, ξ, η) domain, where ξ and η are stream functions of suitably chosen intersecting stream surfaces. The streamline along which these equations are written is defined by the intersection of the stream surface $\xi = \text{const}$ with the stream surface $\eta = \text{const}$. Terms f^s, f^x, f^y, and f^z represent the forces per unit mass acting on the fluid in the s (streamwise), x, y, and z directions, respectively. From this point onwards, we will discuss only Eqs. (1) and (2). The development of Eq. (3) is

similar to that of Eq. (2) and the results for Eq. (3) are given at the appropriate places.

For potential flow without any external forces, f^x and f^y are given in the physical domain (x, y, z) by

$$f^x = -\frac{1}{\rho}\frac{\partial p}{\partial x} \quad \text{and} \quad f^y = -\frac{1}{\rho}\frac{\partial p}{\partial y}, \tag{4}$$

where p is the pressure and ρ is the density. In Eq. (4) the derivatives $\partial/\partial x$ and $\partial/\partial y$ are in the physical (x, y, z) domain. Since $Y(x, \xi, \eta)$ and $Z(x, \xi, \eta)$ are the (y, z) coordinates in the physical domain (x, y, z) of the streamline defined by the intersection of the stream surface $\xi = \text{const}$ with the stream surface $\eta = \text{const}$, the transformation from the (x, ξ, η) domain to the (x, y, z) domain is given by

$$x = x, \quad y = Y(x, \xi, \eta), \quad \text{and} \quad z = Z(x, \xi, \eta), \tag{5}$$

with the metrics of transformation

$$\begin{aligned} \xi_x &= (Y_\eta Z_x - Y_x Z_\eta)/D, & \eta_x &= (Y_x Z_\xi - Y_\xi Z_x)/D, \\ \xi_y &= Z_\eta/D, & \eta_y &= -Z_\xi/D, \\ \xi_z &= -Y_\eta/D, & \eta_z &= Y_\xi/D, \end{aligned} \tag{6}$$

where D, the Jacobian of transformation, is

$$D = (Y_\xi Z_\eta - Z_\xi Y_\eta).$$

Upon transforming the pressure gradients in Eq. (4) from the (x, y, z) domain into the (x, ξ, η) domain, we obtain for f^x and f^y

$$f^x = -(\pi_x + \xi_x \pi_\xi + \eta_x \pi_\eta) U^2 \quad \text{and} \quad f^y = -(\xi_y \pi_\xi + \eta_y \pi_\eta) U^2, \tag{7}$$

where π_x, π_ξ, and π_η are defined as

$$\pi_x = \frac{1}{\rho U^2}\frac{\partial p}{\partial x}, \quad \pi_\xi = \frac{1}{\rho U^2}\frac{\partial p}{\partial \xi}, \quad \text{and} \quad \pi_\eta = \frac{1}{\rho U^2}\frac{\partial p}{\partial \eta}. \tag{8}$$

Derivatives in Eq. (8) are in the (x, ξ, η) domain. With the help of Eq. (8), Eq. (2) becomes

$$Y_{xx} = E[Y_x \pi_x + (Y_x \xi_x - \xi_y)\pi_\xi + (Y_x \eta_x - \eta_y)\pi_\eta], \tag{9}$$

where we have introduced

$$E = 1 + Y_x^2 + Z_x^2.$$

To obtain the continuity equation in the (x, ξ, η) domain, we equate the discharge (volume flow rate) through a cross-stream area element $dy\,dz$ in the

(x, y, z) domain to the discharge through the corresponding area element $d\xi\, d\eta$ in the (x, ξ, η) domain and thus obtain

$$\frac{U}{\sqrt{E}}\, dy\, dz = d\xi\, d\eta = \frac{dy\, dz}{D},$$

which yields

$$U = \sqrt{E}/D. \tag{10}$$

Equation (10) can be obtained, as by Pearson [4], by formal transformation of the continuity equation from the (x, y, z) domain into the (x, ξ, η) domain. Because the present parameters ξ and η are defined differently from Pearson's α and β, the multiplicative factor $C(\alpha, \beta)$ which appears on the right-hand side of Pearson's formulation of the continuity equation is absent in Eq. (10). In the present work ξ and η are not just parameters used to differentiate different stream lines. The parameters ξ and η are the *stream functions*. At the flow inlet, after the stream surfaces along which the flow is to be computed are selected, the values of ξ and η for these surfaces are calculated from the inlet velocity distribution. Thus, for flow through a channel, if the lower wall of the channel is taken to be $\xi = 0$, then the value ξ_i for a given stream surface i is set equal to the volume flow rate between the lower wall and the surface i. The advantage of the present approach is that it leads to a simpler form of the continuity equation. The disadvantage is that now the grid in the (x, ξ, η) domain cannot be defined independently of the boundary conditions, but depends upon the stream surfaces selected in the physical domain and the inlet flow conditions.

For steady incompressible potential flow, integration of Eq. (1) yields the Bernouilli equation

$$\frac{U^2}{2} + \frac{p}{\rho} = \text{const along a streamline.} \tag{11}$$

Henceforth, we will assume that the constant appearing in the Bernoulli equation (11) is identical for all the streamlines. From Eqs. (10) and (11) we obtain

$$\pi_x = -\frac{E_x}{2E} + \frac{D_x}{D}, \quad \pi_\xi = -\frac{E_\xi}{2E} + \frac{D_\xi}{D}, \quad \text{and} \quad \pi_\eta = -\frac{E_\eta}{2E} + \frac{D_\eta}{D}. \tag{12}$$

Upon substituting from Eqs. (12) into Eq. (9), we get

$$Y_{xx} = E\left\{ Y_x\left[\frac{D_x}{D} - \frac{E_x}{2E}\right] + (Y_x\xi_x - \xi_y)\left[\frac{D_\xi}{D} - \frac{E_\xi}{2E}\right] + (Y_x\eta_x - \eta_y)\left[\frac{D_\eta}{D} - \frac{E_\eta}{2E}\right]\right\}. \tag{13}$$

Similarly, we obtain from Eq. (3)

$$Z_{xx} = E\left\{Z_x\left[\frac{D_x}{D} - \frac{E_x}{2E}\right] + (Z_x\xi_x - \xi_z)\left[\frac{D_\xi}{D} - \frac{E_\xi}{2E}\right] + (Z_x\eta_x - \eta_z)\left[\frac{D_\eta}{D} - \frac{E_\eta}{2E}\right]\right\}. \tag{14}$$

We modify Eq. (13) by eliminating the terms involving D_η and E_η (i.e., the terms arising from the π_η term in Eq. (9)) with the help of Eq. (14) and thus obtain

$$DY_\xi Y_{xx} + DZ_\xi Z_{xx} + E D_\xi - D_x F^\xi - \tfrac{1}{2} DE_\xi = 0. \tag{15}$$

where we have introduced

$$F^\xi = Y_x Y_\xi + Z_x Z_\xi. \tag{16}$$

Similarly modifying Eq. (14) with the help of Eq. (13), we get

$$DY_\eta Y_{xx} + DZ_\eta Z_{xx} + E D_\eta - D_x F^\eta - \tfrac{1}{2} DE_\eta = 0, \tag{17}$$

where

$$F^\eta = Y_x Y_\eta + Z_x Z_\eta. \tag{18}$$

Equations (10), (15), and (17) constitute the basic equations of the present approach to the computation of three-dimensional potential flows. Equations (15) and (17) determine the cross-stream coordinates of a given set of streamlines (defined by the chosen values of the parameters ξ and η), and Eq. (10) determines the streamwise velocity along these streamlines. In the next section we present a derivation of Eqs. (15) and (17) from different considerations; and, in the section following that, we present a solution technique for these equations.

III. Stream Surface Equations from Circulation

In this section we present a derivation of Eqs. (15) and (17) from circulation considerations. For a fixed value of η, say η_0, the equations

$$x = x, \quad y = Y(x, \xi, \eta_0), \quad \text{and} \quad z = Z(x, \xi, \eta_0), \tag{19}$$

describe a surface with x and ξ as the parameters. We will refer to this as the x-ξ stream surface, or simply as the x-ξ surface. Consider a closed contour made up of $\xi = \text{const}$ and $x = \text{const}$ lines drawn on the x-ξ surface as shown in Fig. 1. In Fig. 1, ω, the angle between the $x = \text{const}$ line and the $\xi = \text{const}$ line, is given by

$$\cos\omega = \frac{F^\xi}{\sqrt{E}\sqrt{G^\xi}},$$

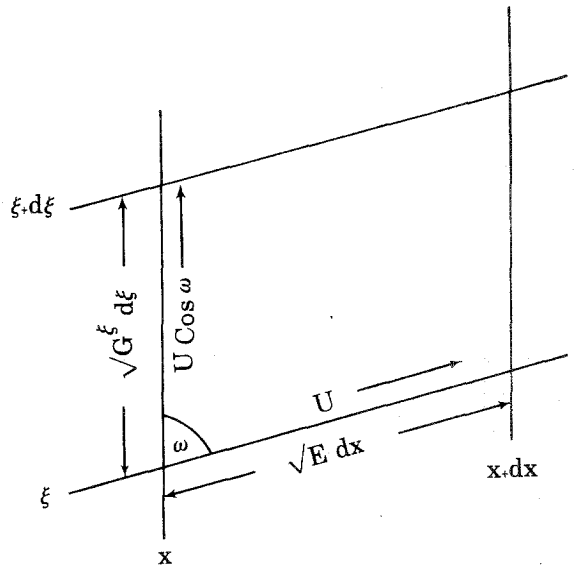

FIG. 1. Contour for the calculation on the x-ξ stream surface.

where E, F^{ξ}, and G^{ξ} are the coefficients of the first fundamental form of the x-ξ surface (see, Stoker [16]). Quantities E and F^{ξ} have been defined previously, and G^{ξ} is given by the formula

$$G^{\xi} = Y_{\xi}^2 + Z_{\xi}^2.$$

The line integrals of the velocity along the $\xi = \text{const}$ and $x = \text{const}$ line elements are respectively given by

$$U\sqrt{E}\,dx = \frac{\sqrt{E}}{D}\sqrt{E}\,dx = \frac{E}{D}\,dx, \tag{20a}$$

$$U\cos\omega\sqrt{G^{\xi}}\,d\xi = \frac{\sqrt{E}}{D}\frac{F^{\xi}}{\sqrt{E}\sqrt{G^{\xi}}}\sqrt{G^{\xi}}\,d\xi = \frac{F^{\xi}}{D}\,d\xi. \tag{20b}$$

The line integrals of the velocity along the $\xi + d\xi = \text{const}$ and $x + dx = \text{const}$ line segments are obtained from (20a) and (20b) by the use of Taylor series expansions. Upon adding the four integrals and simplifying the sum, we obtain for $d\Gamma_{\eta}$, the circulation around the contour, viz.

$$d\Gamma_{\eta} = \left[\frac{\partial}{\partial x}\left(\frac{F^{\xi}}{D}\right) - \frac{\partial}{\partial \xi}\left(\frac{E}{D}\right)\right] dx\,d\xi. \tag{21}$$

For potential flow $d\Gamma_\eta = 0$, and Eq. (21) yields

$$\frac{\partial}{\partial x}\left(\frac{F^\xi}{D}\right) - \frac{\partial}{\partial \xi}\left(\frac{E}{D}\right) = 0. \tag{22a}$$

It can be easily seen that Eq. (22a) is equivalent to Eq. (15). Similarily, by setting the circulation on the x-η surface equal to zero, we obtain

$$\frac{\partial}{\partial \eta}\left(\frac{E}{D}\right) - \frac{\partial}{\partial x}\left(\frac{F^\eta}{D}\right) = 0. \tag{22b}$$

Equation (22b) is equivalent to Eq. (17). To complete the development of this section, we also present the equation obtained by setting the circulation in the cross-stream plane equal to zero

$$\frac{\partial}{\partial \xi}\left(\frac{F^\eta}{D}\right) - \frac{\partial}{\partial \eta}\left(\frac{F^\xi}{D}\right) = 0. \tag{22c}$$

By introducing a stream surface vector, Σ, with components E/D, F^ξ/D, and F^η/D along x, ξ, and η, respectively, Eqs. (22) are rewritten as

$$\nabla \times \Sigma = 0, \tag{23}$$

where ∇ is operator with $\partial/\partial x$, $\partial/\partial \xi$, and $\partial/\partial \eta$ in the x, ξ, and η directions, respectively.

For compressible flow the continuity equation in the (x, ξ, η) domain is obtained by equating the mass flow rate through a cross-stream area element $dy\,dz$ in the (x, y, z) domain to the mass flow rate through the corresponding area element $d\xi\,d\eta$ in the (x, ξ, η) domain, where ξ and η are now associated with the mass flow rates; we thus obtain

$$\frac{\rho U}{\sqrt{E}}\,dy\,dz = d\xi\,d\eta = \frac{dy\,dz}{D}, \tag{24}$$

which yields

$$U = \sqrt{E}/\rho\, D. \tag{25}$$

Proceeding as in the case of incompressible flow, we obtain as the stream surface equations for the compressible flow

$$\nabla \times (\Sigma/\rho) = 0. \tag{26}$$

Before proceeding to the solution of the stream surface equations (15) and (17), we digress briefly to discuss Eq. (26). From Eq. (26) we note that the vector field Σ/ρ is irrotational, and thus it can be described by a potential φ such that

$$\Sigma = \rho\, \nabla\varphi. \tag{27}$$

By integrating the x-component of Eq. (27)

$$\varphi_x = E/\rho\, D = (\sqrt{E}/\rho\, D)\sqrt{E} = U\sqrt{E}, \tag{28}$$

from 0 to 1, we obtain

$$\varphi_1 - \varphi_0 = \int_0^1 U\sqrt{E}\, dx = \int_0^1 U\, ds, \tag{29}$$

where, recall, s is the streamwise distance. Thus, we note that φ represents the usual velocity potential. The import of the second component of Eq. (27) is seen by integrating it between two neighboring streamlines on an x-ξ surface. The result is the well-known result that a line drawn normal to a streamline is an equipotential line. A similar result is obtained from the third component of Eq. (27).

IV. Solution of the Stream Surface Equations

In this section we present a technique for the solution of the stream surface equations (15) and (17) in the case of internal flows. The solution technique presented assumes that the streamlines do not cross over from one wall to another, and thus, is limited to flows without any axial swirl. By writing out the D_ξ term in Eq. (15) and the D_η term in Eq. (17), we rewrite these equations as

$$DY_\xi Y_{xx} + DZ_\xi Z_{xx} + E(Y_{\xi\xi} Z_\eta + Y_\xi Z_{\eta\xi} - Y_{\eta\xi} Z_\xi - Y_\eta Z_{\xi\xi}) - D_x F^\xi - \tfrac{1}{2} DE_\xi = 0 \tag{30}$$

$$DY_\eta Y_{xx} + DZ_\eta Z_{xx} + E(Y_{\xi\eta} Z_\eta + Y_\xi Z_{\eta\eta} - Y_{\eta\eta} Z_\xi - Y_\eta Z_{\xi\eta}) - D_x F^\eta - \tfrac{1}{2} DE_\eta = 0. \tag{31}$$

We label the grid along x, ξ, and η by i, j, and k, respectively. Let Δx, $\Delta\xi$, $\Delta\eta$ respectively represent uniform grid spacings along x, ξ, and η. By finite differencing Y_{xx}, Z_{xx}, $Y_{\xi\xi}$, and $Z_{\xi\xi}$ using the central difference approximation, we obtain from Eq. (30)

$$a_y Y_{i,j,k} + b_y Z_{i,j,k} = c_y, \tag{32}$$

where

$$a_y = \frac{2DY_\xi}{\Delta x^2} + \frac{2EZ_\eta}{\Delta\xi^2}, \quad b_y = \frac{2DZ_\xi}{\Delta x^2} - \frac{2EY_\eta}{\Delta\xi^2},$$

$$c_y = \frac{DY_\xi}{\Delta x^2}(Y_{i+1,j,k} + Y_{i-1,j,k}) + \frac{DZ_\xi}{\Delta x^2}(Z_{i+1,j,k} + Z_{i-1,j,k}) + \frac{EZ_\eta}{\Delta\xi^2}(Y_{i,j+1,k} + Y_{i,j-1,k}) - \frac{EY_\eta}{\Delta\xi^2}(Z_{i,j+1,k} + Z_{i,j-1,k}) + E(Y_\xi Z_{\xi\eta} - Z_\xi Y_{\xi\eta}) - D_x F^\xi - \tfrac{1}{2} DE_\xi.$$

Proceeding similarly, we get from Eq. (31)

$$a_z Y_{i,j,k} + b_z Z_{i,j,k} = c_z, \tag{33}$$

where

$$a_z = \frac{2DY_\eta}{\Delta x^2} - \frac{2EZ_\xi}{\Delta \eta^2}, \quad b_z = \frac{2DZ_\eta}{\Delta x^2} + \frac{2EY_\xi}{\Delta \eta^2},$$

$$c_z = \frac{DY_\eta}{\Delta x^2}(Y_{i+1,j,k} + Y_{i-1,j,k}) + \frac{DZ_\eta}{\Delta x^2}(Z_{i+1,j,k} + Z_{i-1,j,k})$$

$$- \frac{EZ_\xi}{\Delta \eta^2}(Y_{i,j,k+1} + Y_{i,j,k-1}) + \frac{EY_\xi}{\Delta \eta^2}(Z_{i,j,k+1} + Z_{i,j,k-1})$$

$$+ E(Z_\eta Y_{\xi\eta} - Y_\eta Z_{\xi\eta}) - D_x F^\eta - \tfrac{1}{2} DE_\eta.$$

The solution of Eqs. (32) and (33) is carried out in two parts: (i) solution on the surface of the duct walls and (ii) solution in the interior region of the duct. These two solutions are carried out iteratively in tandem. Let us consider flow through a duct as shown in Fig. 2. The four duct walls are labeled N (North), S (South), E (East), and W (West).

"WALL SURFACE" SOLUTION. We start with E–W walls. We note that the E–W

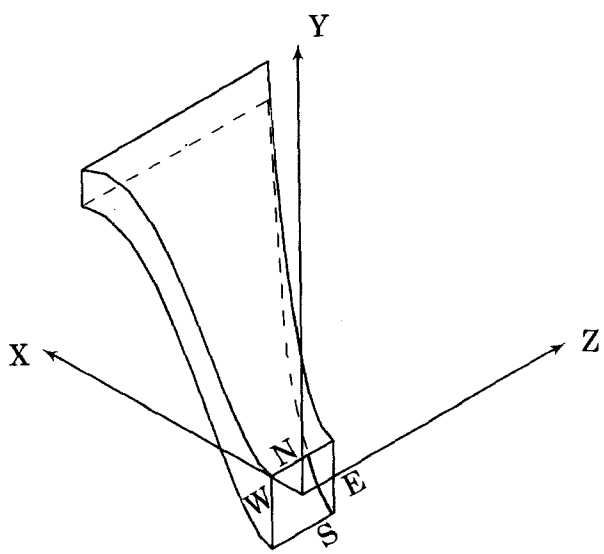

FIG. 2. The N, S, E, W labeling convention employed to identify the duct walls. The duct shown in the figure corresponds to the first sample computation.

walls are x-ξ surfaces, and are thus described by Eq. (32). Upon solving for $Y_{i,j,k}$ from Eq. (32) we obtain

$$Y_{i,j,k} = (c_y - b_y Z_{i,j,k})/a_y, \tag{34}$$

where $k = 1$ for the E wall, and $k = k_{\max}$ for the W wall. All the derivatives of Y appearing on the right-hand side of Eq. (34) (via the definitions of a_y, b_y, and c_y) are centrally differenced; note that none of the resulting finite differences contain $Y_{i,j,k}$. All the derivatives of Z involving η are differenced using forward differencing on the E wall and backward differencing on the W wall. All the other derivatives of Z are centrally differenced. Boundary conditions for Eq. (34) are specified as follows: along the $i = 1$ edge of the wall (see, Fig. 3, which shows the W wall), Y is specified to match the inlet flow conditions; along the $j = 1$ and $j = j_{\max}$ edges, Y is determined from the given wall geometry; along the $i = i_{\max}$ edge we specify Y to match the given or assumed exit flow conditions.

With the value of Y thus specified all around the edges, Eq. (34) is solved for $Y_{i,j,1}$ and the for $Y_{i,j,k_{\max}}$ for $i = 2, \ldots, (i_{\max} - 1), j = 2, \ldots, (j_{\max} - 1)$ using the method of successive displacement. During the solution of Eq. (34), Z is considered known (from the previous iteration or from the assigned starting values). After Eq. (34) is solved for $Y_{i,j,1}$, values of $Z_{i,j,1}$ are determined from the newly calculated $Y_{i,j,1}$ to satisfy the given W wall surface equation; and after Eq. (34) is solved for $Y_{i,j,k_{\max}}$, values $Z_{i,j,k_{\max}}$ are determined from the newly calculated $Y_{i,j,k_{\max}}$ to satisfy the given E wall surface equation.

The N-S walls are x-η surfaces and are described by Eq. (33). Upon solving for $Z_{i,j,k}$ from Eq. (33) we obtain

$$Z_{i,j,k} = (c_z - a_z Y_{i,j,k})/b_z, \tag{35}$$

where $j = 1$ for the S wall and $j = j_{\max}$ for the N wall. The finite differencing,

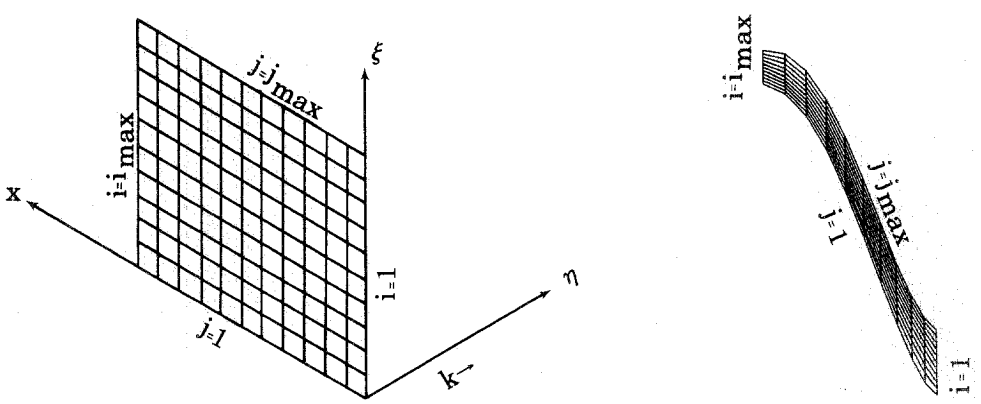

FIG. 3. West wall in the computational domain (left) and in the physical domain (right).

specification of the boundary conditions, and the solution of Eq. (35) is carried out similarly to that employed in solving Eq. (34). Now, after Eq. (35) is solved for Z, values of Y on the surface of the walls are calculated to satisfy the given N–S walls surface equations.

"INTERIOR REGION" SOLUTION. All the derivatives appearing in a_y, b_y, c_y, a_z, b_z, and c_z in Eqs. (32) and (33) are approximated using the central differencing. We note that none of the resulting finite difference approximations contain $Y_{i,j,k}$ or $Z_{i,j,k}$. At the duct inlet, $i=1$, Y and Z are specified to match the inlet flow conditions. At the exit, $i=i_{\max}$, Y and Z are specified to meet the given or the assumed exit flow conditions. Values of Y and Z on the surface of the walls are those calculated in the "wall surface" solution step. With the boundary conditions thus specified, Eqs. (32) and (33) are solved at the interior grid points by the method of successive displacement. At any given grid point, Eqs. (32) and (33) are solved simultaneously for $Y_{i,j,k}$ and $Z_{i,j,k}$.

The algorithm used for the following sample computations is summarized as:

(i) With the duct geometry specified, generate the starting values of Y and Z assuming the flow is uniform throughout;

(ii) carry out the "wall surface" solutions for the E, W, S, and N walls;

(iii) carry out the "interior region" solution;

(iv) repeat the sequence of steps (ii) and (iii) until the desired convergence is obtained.

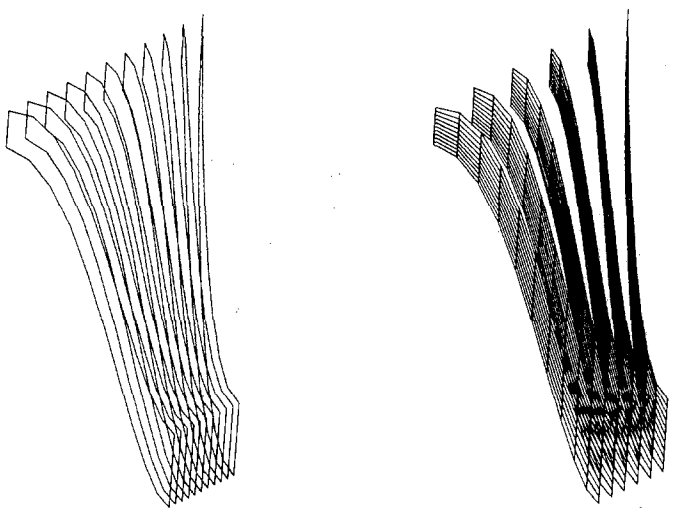

FIG. 4. Results of the first sample computations: left—boundaries of the x-ξ stream surfaces; right—details of every other x-ξ stream surface.

The first sample computation is of flow through an offset rectangular duct with 1.0×1.0 inlet and 3.0×0.5 exit (see Fig. 2). With the origin of the coordinate system placed at the center of the inlet section, the duct walls are specified as

$$Y_N = 0.5 - 0.0625x^2 + 2\left[1 - \cos\left(\frac{\pi x}{2}\right)\right],$$

$$Y_S = -0.5 + 0.0625x^2 + 2\left[1 - \cos\left(\frac{\pi x}{2}\right)\right],$$

$$Z_E = 0.5 + 0.25x^2,$$

$$Z_W = -0.5 - 0.25x^2,$$

where the subscript N, S, E, or W identifies the corresponding wall. Computations were carried out over the domain

$$0 \leqslant \xi \leqslant 1, \quad 0 \leqslant \eta \leqslant 1, \quad \text{and} \quad 0 \leqslant x \leqslant 2,$$

with uniform grid spacing

$$\Delta\xi = 0.1, \quad \Delta\eta = 0.1, \quad \text{and} \quad \Delta x = 0.2.$$

Thus, the computations were carried out with 11 x-ξ stream surfaces (including the E–W walls), and 11 x-η stream surfaces (including the N–S walls), which gives a

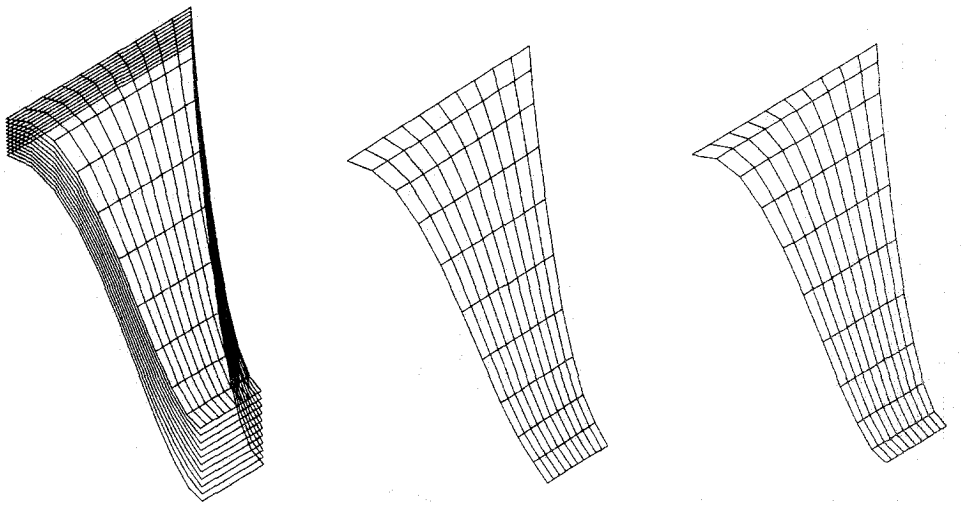

FIG. 5. Results of the first sample computations: left—boundaries of the x-η stream surfaces and the details of the N wall surface; center—details of the sixth from the top x-η stream surface; right—details of the S wall stream surface.

total of 121 streamlines. The inlet and the exit flow conditions were assumed to be uniform. The convergence criterion used to terminate the iterative calculations was

$$\left\{ \sum_{i,j,k} [(Y_{i,j,k}^{n+1} - Y_{i,j,k}^{n})^2 + (Z_{i,j,k}^{n+1} - Z_{i,j,k}^{n})^2] \right\}^{1/2} \leqslant 10^{-3}, \tag{36}$$

where the superscript n represents the iteration number.

A single figure showing all of the 121 computed streamlines becomes too encumbered to convey anything meaningful; thus, the results are presented selectively in Figs. (4)–(6). On the left in Fig. 4 are shown the boundaries of all the 11 x-ξ surfaces, and, on the right, details (in terms of the streamlines and the $x = \text{const}$ lines) of every other of these surfaces. Figure 5 shows, from the left to right, (i) boundaries of all of the 11 x-η surfaces and details of the N wall surface, (ii) details of the sixth from the top x-η surface, and (iii) details of the S wall surface. To show the inter-relationship of the x-ξ and the x-η surfaces, in Fig. 6 we have shown two of the x-ξ and two of the x-η stream surfaces in the same figure. Please note, only the 12 boundary lines shown in Fig. 2 (9 as solid and 3 as broken) are specified by the duct geometry. All the other streamlines shown on the wall surfaces in these figures were calculated as part of the computations.

It took 54 iterations for convergence. The computations were carried out on an IBM 3081 VM/CMS, and took 5.2s CPU time. Reducing the convergence criterion from 10^{-3} to 5×10^{-4} increased the required number of iterations to 89 and the CPU time to 8.4s.

For the duct considered in the first sample computations, at a fixed value of x, Z was constant along the E–W walls, and Y was constant along the N–S walls; thus, we needed to solved only for Y on the surfaces of E–W walls, and only for Z on the

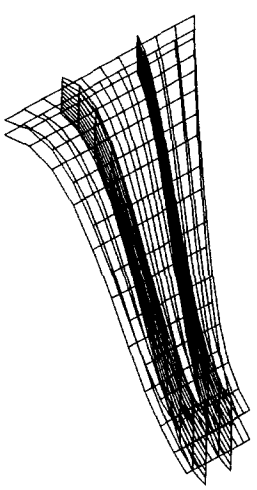

FIG. 6. Results of the first sample computations: Two of the x-ξ and two of the x-η stream surfaces.

surfaces of N–S walls. As the second sample computations, we have selected a duct for which it is necessary to solve for both Y and Z on each of the wall surfaces. We consider flow through a straight duct whose cross section changes from a 1×1 square to a rhombus of continuously decreasing minor axis along the flow (see, Fig. 7). With the origin of the coordinate system placed at the center of the inlet section, the ducts wall are specified as

$$Z_W = (y-r)s - r; \qquad -\frac{1}{4r} \leqslant y \leqslant r, \tag{37a}$$

$$Z_E = (y+r)s + r; \qquad -r \leqslant y \leqslant \frac{1}{4r}, \tag{37b}$$

$$Y_S = (z-r)s - r; \qquad -\frac{1}{4r} \leqslant z \leqslant r, \tag{37c}$$

$$Y_N = (z+r)s + r; \qquad -r \leqslant z \leqslant \frac{1}{4r}, \tag{37d}$$

where,

$$s = \frac{1-4r^2}{1+4r^2}.$$

The parameter r, which is $1/\sqrt{2}$ times the semi-minor axis, was taken to vary as $x/2$.

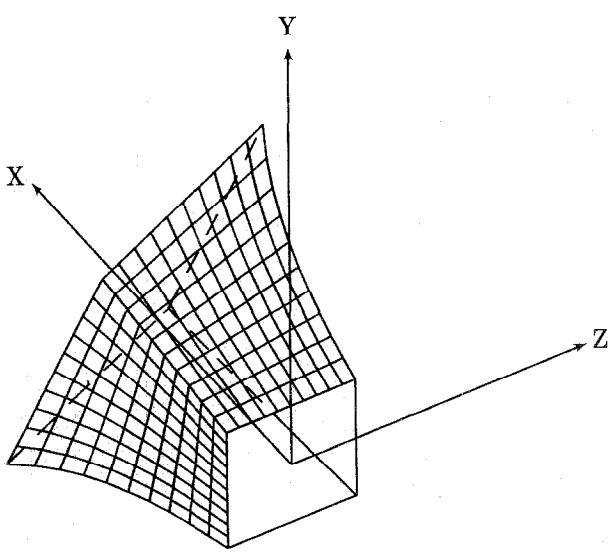

FIG. 7. Duct for the second sample computations, including the computed streamlines along the W and N wall surfaces.

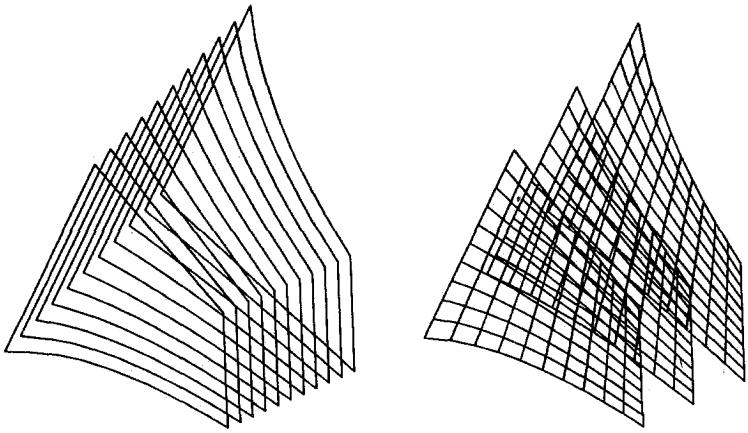

FIG. 8. Results of the second sample computations: left—boundaries of all of the x-ξ stream surfaces; right—details of second, sixth, and tenth from the W wall x-ξ stream surface.

In these sample computations, after Eq. (33) is solved for $Y_{i,j,1}$ (i.e., for the W wall), Eq. (37a) is then used to calculate $Z_{i,j,1}$. Equations (37b), (37c), and (37d) were used similarly in the "wall surface" computations. Computations were carried out over the domain

$$0 \leqslant \xi \leqslant 1, \qquad 0 \leqslant \eta \leqslant 1, \quad \text{and} \quad 0 \leqslant x \leqslant 1,$$

with uniform grid spacing

$$\Delta\xi = 0.1, \qquad \Delta\eta = 0.1, \qquad \text{and} \qquad \Delta x = 0.1.$$

In Fig. 7 are shown the computed streamlines along the N and W wall surfaces. In Fig. 8, on the left are shown the boundaries of all the 11 x-ξ stream surfaces, and on the right details of second, sixth, and tenth stream surfaces from the W wall. As can be inferred from the geometry of the duct, the x-η surfaces are similar to the x-ξ surfaces, and are, thus, not shown for the sake for brevity. It took 26 iterations and 2.6s of CPU time to meet the convergence criterion given in Eq. (36).

V. CONCLUSIONS

A new approach is presented for the calculation of three-dimensional incompressible potential flows. In this approach, the streamline coordinates in the cross-stream plane are calculated as part of the dependent variables. The results thus provide directly the streamline geometry, which can be used as a boundary-fitted grid for the computation of three-dimensional viscous flows. In the "partially parabolic" approach to the computation of viscous flows, as for example, in Briley and McDonald (17), and Towne and Hoffman (18), one needs, as an input to the

"partially parabolic" calculations, the pressure field calculated with the potential flow approximation. The method presented in this paper, besides providing a boundary-fitted grid, also provides the potential flow pressure field. After Y and Z are calculated, Eq. (10) can be used to calculate U, which in turn will yield the pressure field when substituted into the Bernoulli equation. The pressure field thus calculated is for incompressible flows.

ACKNOWLEDGMENTS

We thank Dr. James M. Bowyer and Dr. Paul O. Steranka for their careful reading of the manuscript. The work was partially supported by the U.S. Army Research Office Grant DAAL 03-87-G-0003.

REFERENCES

1. A. H. SHAPIRO, *The Dynamics and Thermodynamics of Compressible Fluid Flow* (Wiley, New York, 1953), Vol. 1, p. 336.
2. S. UCHIDA AND M. YASUHARA, *J. Aeronaut. Sci.* **23**, 830 (1956).
3. R. ISHII, *Trans. Japan Soc. Aeronaut. Space Sci.* **23**, 18 (1980).
4. C. E. PEARSON, *J. Comput. Phys.* **42**, 257 (1981).
5. C. E. PEARSON, *Comm. Appl. Num. Methods* **1**, 177 (1985).
6. D. A. ANDERSON, J. C. TANNEHILL, AND R. H. PLETCHER, *Computational Fluid Mechanics and Heat Transfer* (McGraw–Hill, New York, 1984), p. 504.
7. S. V. PATANKAR AND D. B. SPALDING, *J. Heat Mass Transfer* **10**, 1389 (1967).
8. O. K. KWON AND R. H. PLETCHER, *ASME Trans. J. Fluid Eng.* **108**, 64 (1986).
9. U. GHIA, K. N. GHIA, S. G. RUBIN, AND P. K. KHOSLA, *Comput. Fluids* **9**, 123 (1981).
10. R. MEYDER, *J. Comput. Phys.* **17**, 53 (1975).
11. C. FARREL AND J. ADAMCZYK, *ASME Trans. J. Power Eng.* **104**, 143 (1982).
12. J. F. THOMPSON, Z. U. A. WARSI, AND C. W. MASTIN, *J. Comput. Phys.* **47**, 1 (1982).
13. M. S. GREYWALL, *Comput. Methods Appl. Mech. Eng.* **21**, 231 (1980).
14. M. S. GREYWALL, *Comput. Methods Appl. Mech. Eng.* **36**, 71 (1983).
15. M. S. GREYWALL, *J. Comput. Phys.* **59**, 224 (1985).
16. J. J. STOKER, *Differential Geometry* (Wiley-Interscience, New York, 1969), p. 81.
17. W. R. BRILEY AND H. MCDONALD, in *Proceedings, AIAA Computational Fluid Dynamics Conference, Williamsburg, VA, July* 1979, p. 74.
18. C. E. TOWNE AND J. D. HOFFMANN, AIAA Paper 84-0256, January 1984.